Efficient and Stable Large Bandgap $MAPbBr_3$ Perovskite Solar Cell Attaining an Open Circuit Voltage of 1.65 V

Hongwei Zhu,[1,2,3] Linfeng Pan,[4] Felix T. Eickemeyer,[1*] Michael A. Hope,[5] Olivier Ouellette,[1] Anwar Qasem M Alanazi,[1] Jing Gao,[1] Thomas Paul Baumeler,[1] Xianggao Li,[2,3] Shirong Wang,[2,3] Shaik M. Zakeeruddin,[1] Yuhang Liu,[1,*] Lyndon Emsley,[5] and Michael Grätzel[1*]

[1]Laboratory of Photonics and Interfaces (LPI), Institute of Chemical Sciences & Engineering, École Polytechnique Fédérale de Lausanne, Station 6, Lausanne 1015, Switzerland.

[2]School of Chemical Engineering and Technology, Tianjin University, Tianjin 300072, China.

[3]Collaborative Innovation Center of Chemical Science and Engineering, Tianjin 300072, China.

[4]Laboratory of Photomolecular Science (LSPM), Institute of Chemical Sciences & Engineering, École Polytechnique Fédérale de Lausanne, Station 6, Lausanne 1015, Switzerland.

[5]Laboratory of Magnetic Resonance, Institute of Chemical Sciences and Engineering, École Polytechnique Fédérale de Lausanne (EPFL), Lausanne, Switzerland.

[*]Correspondance to: Dr. Yuhang Liu (yuhang.liu@epfl.ch), Dr. Felix T. Eickemeyer (felix.eickemeyer@epfl.ch), and Prof. Michael Graetzel (michael.greatzel@epfl.ch).

ABSTRACT: We report on the preparation of $MAPbBr_3$ perovskite films of high electronic quality by applying a methylamine (MA) vapor treatment and mitigating surface defects using the amphiphilic molecular passivator, neopentylammonium chloride (NPACl). We find that post-treatment of $MAPbBr_3$ with methylamine (MA) vapor effectively smoothens the surface of the perovskite, eliminating unwanted corrugations and producing phase-pure pin-hole free films. The subsequent coating of $MAPbBr_3$ with NPACl eliminates deleterious surface states that act as electron–hole recombination centers while enhancing the resilience of the perovskite solar cell (PSC) against heat stress and ambient moisture, with solid state NMR demonstrating their atomic-scale interaction. As a result, we achieve an unprecedented V_{oc} of 1.65 V which is a record level for mesoporous single junction PSCs together with a power conversion efficiency (PCE) of over 10% in standard AM 1.5 sunlight. The PSC also retains 91.3% of its initial performance after 1100 h light soaking under full sunlight and at 60 °C, while maintaining the device at maximum power point. In contrast, the pristine PSC maintained only 34% of its initial efficiency under the same aging condition.

Over the past decade, metal halide perovskites have been the subject of intense investigations owning to their unique optoelectronic properties.[1-3] The power conversion efficiency (PCE) of perovskite solar cells (PSCs) have increased from less than 4% to 25.5% during this period,[4-7] exceeding the PCE of the market leader multi-crystalline silicon. Current investigations focus on medium-to-low bandgap PSC and use iodide-rich compositions containing up to 20% bromide.[8-12] These devices now routinely achieve PCEs over 20% and open circuit voltages (V_{oc}) of up to 1.2 V. Yet, the compositional and structural versatility of metal halide perovskites endows them with far wider options. In particular, large bandgap perovskites are attractive for tandem solar cells or solar water splitting and CO_2 reduction devices, which require high photovoltages.[13-14] One important large bandgap perovskite material is $MAPbBr_3$ with a bandgap of around 2.3 eV which corresponds to a Shockley-Queisser limit V_{oc} and PCE of 1.98 V and 16.5%, respectively.[15]

At present, many methods are used to improve the open circuit voltage (V_{oc}) and PCE of $MAPbBr_3$-PSCs. Aranda et al.[16] applied lithium ions to passivate the surface of mesoporous TiO_2 and reduced the non-radiative recombination at the $MAPbBr_3/TiO_2$ interface, resulting in a high V_{oc} of 1.58 V. Wu et al.[17] chose the high HOMO acceptor material ICBA for a $MAPbBr_3$-based inverted PSC electron transporting layer (ETL) in combination with solvent annealing, with the device obtaining a high V_{oc} in excess of 1.6 V. More recently, Hu et al.[14] applied a MoO_x layer by e-beam evaporation to reengineer the anode interface between NiOx and $MAPbBr_3$ and an ALD deposited ZrO_2 layer to modify the cathode interface between $PC_{61}BM$ and $MAPbBr_3$. With these complex and expensive additional layer processing they obtained a record V_{oc} of 1.653 V under one sun illumination with a high PCE of 10.08%. Although, the V_{oc} and PCE of $MAPbBr_3$-based PSCs have been effectively improved in their work, the device stability, especially the operational stability under high temperature conditions, remain a challenge.

Here we report a wide band gap methylammonium lead bromide ($MAPbBr_3$)-based mesoporous PSC, where all the active layers have been solution deposited, exhibiting record level V_{oc} of 1.65 V and a PCE over 10% together with outstanding operational stability with all active layer solution processed. We achieve an outstanding operational stability under 1100 hours of simulated 1-sun illumination at 60 °C temperature.

The fast crystallization of $MAPbBr_3$ is known to impose challenges for depositing high quality $MAPbBr_3$ films from solution.[18] To address this issue, we treat the $MAPbBr_3$ with methylamine (MA) vapor resulting in effective smoothening of the highly corrugated surface of as-prepared films.[19] We use top-view and cross-sectional scanning electron microscopy (SEM) measurements to confirm the improvement of the perovskite film morphology. UV-*vis* absorption spectra also reveal the suppression of voids upon MA vapor treatment, resulting in a better transparency. For a MA vapor treated $MAPbBr_3$-based PSC we achieve a PCE of 9.3%. In contrast, the PCE of the control device without MA vapor treatment is 6.2%. Furthermore, the MA vapor treated $MAPbBr_3$ perovskite film is subsequently surface coated with neopentylammonium chloride (NPACl). Due to its amphiphilic character NPACl assumes a dual function: the polar ammonium head groups insert into A-site cation vacancy defects present at perovskite layer surface, while the hydrophobic umbrella-shaped neopentyl tail establishes an intimate contact with the hole conductor and protects the perovskite layer from being attacked by water molecules. In this fashion NPACl boosts both the efficiency and stability of the PSC.

MA vapor post-treatment is an effective defect-healing method to fabricate high-quality perovskite films.[20-22] We deposited the $MAPbBr_3$ film using a one-step anti-solvent method, followed by applying the MA vapor post treatment as previously reported.[19] UV-*vis* absorbance spectra of the perovskite films with and without MA vapor post-treatment, measured with and without an integrating sphere, are shown in **Figure S1** which shows the typical excitonic absorption onset at 540 nm. The measurement without an integrating sphere shows a large background signal at wavelengths above 540 nm for the pristine $MAPbBr_3$ perovskite which is due to light scattering.[23] The morphologies of the $MAPbBr_3$ perovskite with and without MA vapor treatment are characterized by cross-sectional and top-view SEM measurements, and the results are shown in **Figure 1**. The $MAPbBr_3$ film without MA vapor post-treatment shows pinholes at the surface and gaps between the perovskite and TiO_2, which are absent in the MA treated films. This is the reason for the pronounced light scattering in the untreated $MAPbBr_3$ film. The bandgap of $MAPbBr_3$ is estimated to be 2.32 eV as determined from the inflection point of the incident photon to current conversion efficiency (IPCE) spectrum[24] (**Figure S2**).

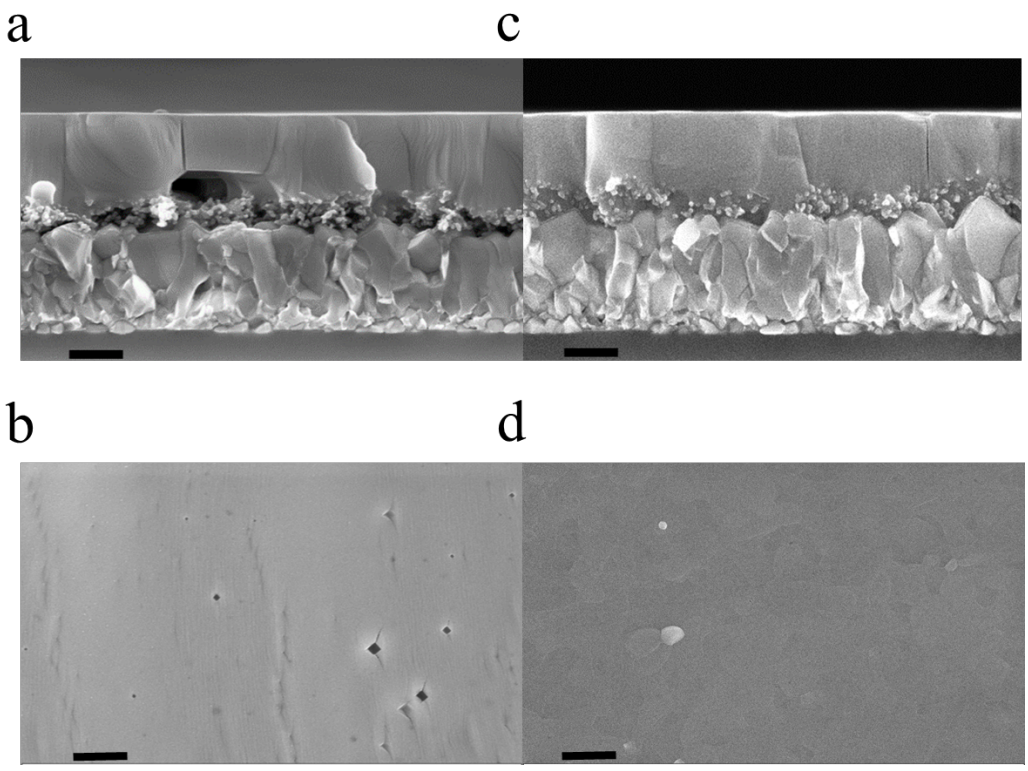

Figure 1. (a) and (b), cross-section and top-view SEM images of $MAPbBr_3$ films without MA vapor post-treatment, (c) and (d), cross-sectional and top-view SEM images of $MAPbBr_3$ films with MA vapor post-treatment. All scale bars are 200 nm.

To verify the effect of MA vapor post-treatment on PSC performance, we fabricated n-*i*-p solar cell devices with the layered device structure: FTO/compact TiO_2/mesoscopic TiO_2/$MAPbBr_3$ /HTL/Au. *J-V* curves of the best performing PSC subjected to MA vapor treatment, denoted as perovskite/MA, achieved a PCE of 9.27% with a J_{sc} of 8.3 mA/cm^2, a V_{oc} of 1.58 V and a fill factor (FF) of 67.4% (**Figure 4a** and **Table S1**). On the contrary, PSCs based on pristine perovskite without MA vapor treatment yield PCE of ~ 6% (**Figure 4a** and **Table 1**). We measured the absolute photon flux associated with the photoluminescence (PL) for $MAPbBr_3$ films with and without MA vapor treatment, and the results are shown in **Figure S3**. Compared to the pristine $MAPbBr_3$ film, an improved PL quantum yield (PLQY) is observed for the $MAPbBr_3$ film with MA vapor treatment, indicating a suppressed recombination for the MA post-treated sample.[25]

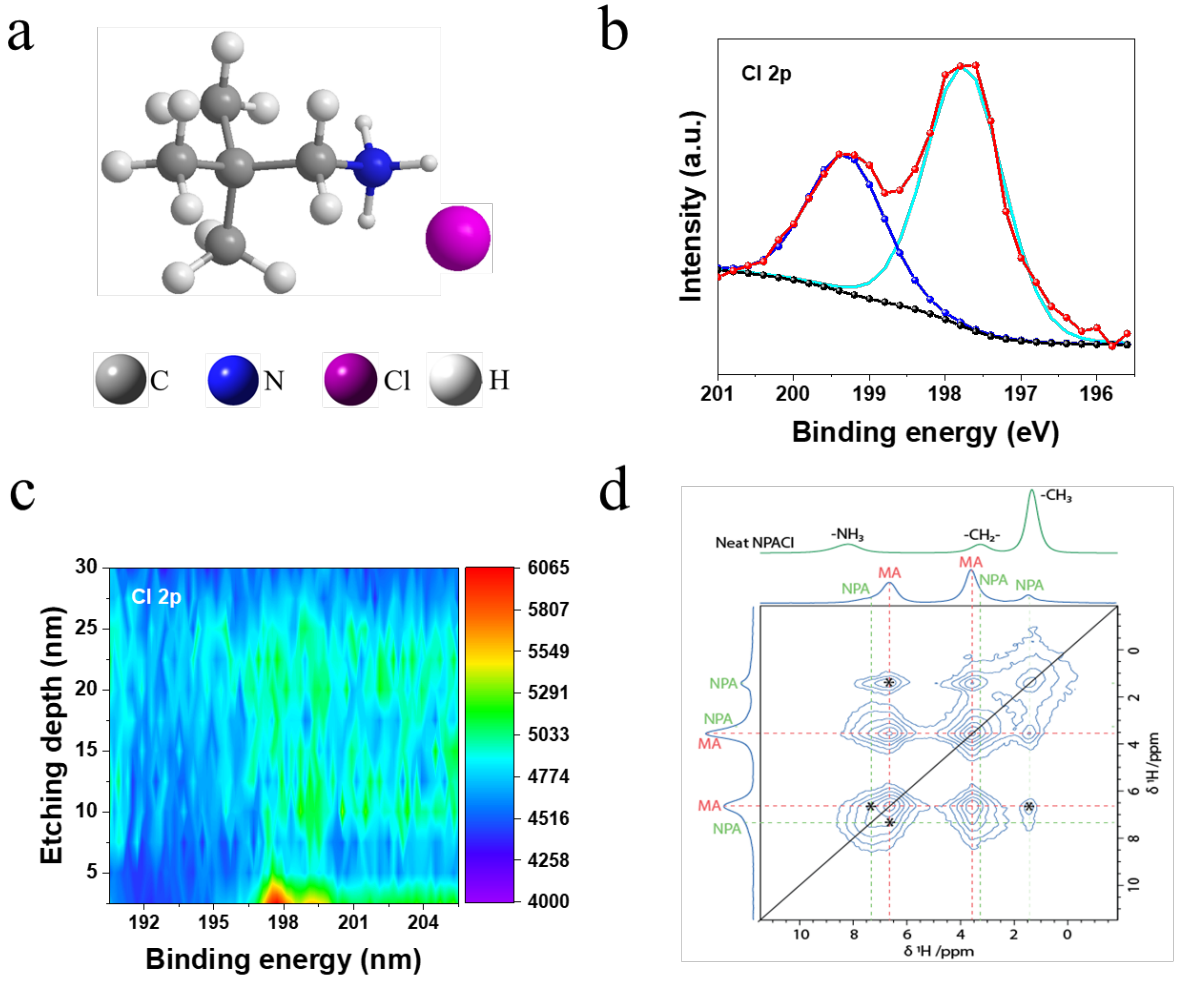

Figure 2. (a), Chemical structure of NPACl. (b), High-resolution deconvoluted Cl 2p XPS spectra for perovskite/NPACl film. (c), Cl 2p XPS depth profiles of the perovskite/NPACl film. (d), ^{1}H–^{1}H spin-diffusion NMR spectrum of $MAPbBr_3$ mechanosynthesised with 1 mol% NPACl, using a 1 s mixing time, and the 1D spectrum of neat NPACl; the asterisks highlight distinct cross peaks between NPA and MA.

We modified the surface of MA-vapor treated $MAPbBr_3$ films with neopentylammonium chloride (NPACl) whose structure is shown in **Figure 2a**. We casted the NPACl by spin coating on the surface of $MAPbBr_3$ using a solution of 3 mg/mL NPACl in *iso*-propanol. Surface and depth X-ray photoelectron spectroscopy (XPS) profiling were used to characterize the thickness of the NPACl film and the chemical environments in the perovskite layers with and without NPACl passivation, and the results are shown in **Figures 2b**, **2c** and **S4**. The Cl 2p peak appearing at the

perovskite/NPACl film surface is attributed to NPACl. From the Cl 2p XPS depth profiling we estimate the thickness of the NPACl layer to be ~4 nm (**Figure 2c**); note that no Cl incorporation in the perovskite is observed by XRD, UV–*vis*, or PL measurements (vide infra), therefore the Cl signal is ascribed solely to the NPACl layer. UV-*vis* measurements showed that the NPACl treatment did not affect the optical transmission of the $MAPbBr_3$ film (**Figure S5**).

To prove the atomic-scale interaction of NPACl with $MAPbBr_3$, we measured ^1H–^1H spin-diffusion MAS NMR spectra[26] for $MAPbBr_3$ mechano-synthesized with 1 mol% NPACl (**Figure 2d**). In a spin-diffusion spectrum, cross peaks are only observed between dipolar coupled species that must therefore be in close proximity, which has previously been exploited to determine the mode of operation of different passivating agents in hybrid perovskite systems.[27-29] There is some overlap between the ^1H signals of MA and NPA, but cross peaks between MA and NPA can nevertheless be distinguished (marked by asterisks), categorically demonstrating that the two cations must be present within ~ 1 nm of each other (given the 1 s mixing time). The identification of the cross peaks is corroborated by varying the mixing time, which differentiates intramolecular NPA–NPA spin diffusion and intermolecular NPA–MA spin diffusion (**Figure S6**). A change in the local environment of the NPA -NH_3 group can also be seen from the change in ^1H shift from 8.2 ppm to 7.1 ppm; this is consistent with passivation of A-site vacancies, which significantly changes the local environment of the ammonium headgroup.[28, 30] The X-ray diffraction (XRD) patterns of the pristine $MAPbBr_3$ perovskite, perovskite/MA and perovskite/MA with NPACl surface coating (denoted as perovskite/MA/NPACl) films are shown in **Figure 3a**. All diffractograms show two sharp diffraction peaks at 15.0 °, 30.2 ° and a relatively weaker peak at 45.9 °, which can be assigned to (0 0 1), (0 0 2) and (0 0 3) planes of the $MAPbBr_3$ perovskite crystal, respectively.[31] The improved diffraction intensity for the perovskite films based on MA vapor treatment implies better $MAPbBr_3$ perovskite crystal quality. No new diffraction peak is observed for the perovskite/MA/NPACl film, proving that NPACl cannot enter the lattice of the perovskite, presumably due to the large cationic size.

Figure 3b shows the time-resolved photoluminescence TRPL measurements of the perovskite films on FTO glass/TiO_2 substrates for pristine perovskite, perovskite/MA and perovskite/MA/NPACl. The measurements exhibit two distinctly different characteristics: a very fast decay within the first few nanoseconds and a much slower decay which becomes mono-

exponential at later times. To understand the fast initial decay, we have to consider several potential mechanisms. $MAPbBr_3$ has a charge carrier mobility > 10 cm^2/Vs[32] which leads to a diffusion-controlled spatial equilibration of the exponential charge carrier density profile right after the laser pulse excitation within less than 1 ns. Thus, carrier diffusion is not observed with the time resolution of around 1 ns of our TRPL measurement. In our experiment we use laser fluences < 5 nJ/cm^2 which are very low so that radiative and Auger recombination are negligible negligible.[33] Hence, we attribute the fast decay within the first few nanoseconds to electron injection into the mesoporous TiO_2 layer. This charge transfer ceases when equilibrium is reached between the electron quasi-Fermi levels in the perovskite and the TiO_2 layer.[34] The slow PL decay at later times has two origins: bulk and interface charge carrier recombination and charge back-injection from TiO_2 into the perovskite layer. We follow the work of Krückemeier et al.[34] and plot the differential lifetime $\tau_{TRPL} = \left(-\frac{1}{2}\frac{d\ \ln \Phi_{TRPL}}{dt}\right)^{-1}$ in **Figure S7**. τ_{TRPL} is the mono-exponential TRPL decay time constant (lifetime) at each delay time. The fast initial drop is reflected by the very short lifetimes at early times (first few nanoseconds), while at later times the lifetimes reach a plateau. The MA-treated samples exhibit a nearly one order of magnitude higher lifetime compared to the untreated sample. This is a clear indication of strongly reduced trap-assisted non-radiative bulk and interface recombination, which is not surprising since the crystal quality is improved with the MA treatment. The higher lifetime of the perovskite/MA/NPACl sample compared to the perovskite/MA sample can be attributed to a reduced non-radiative recombination rate at the perovskite surface since the bulk perovskite layer is the same for both cases and the only difference is the NPACl surface passivation. This demonstrates the beneficial effect of the NPACl treatment.

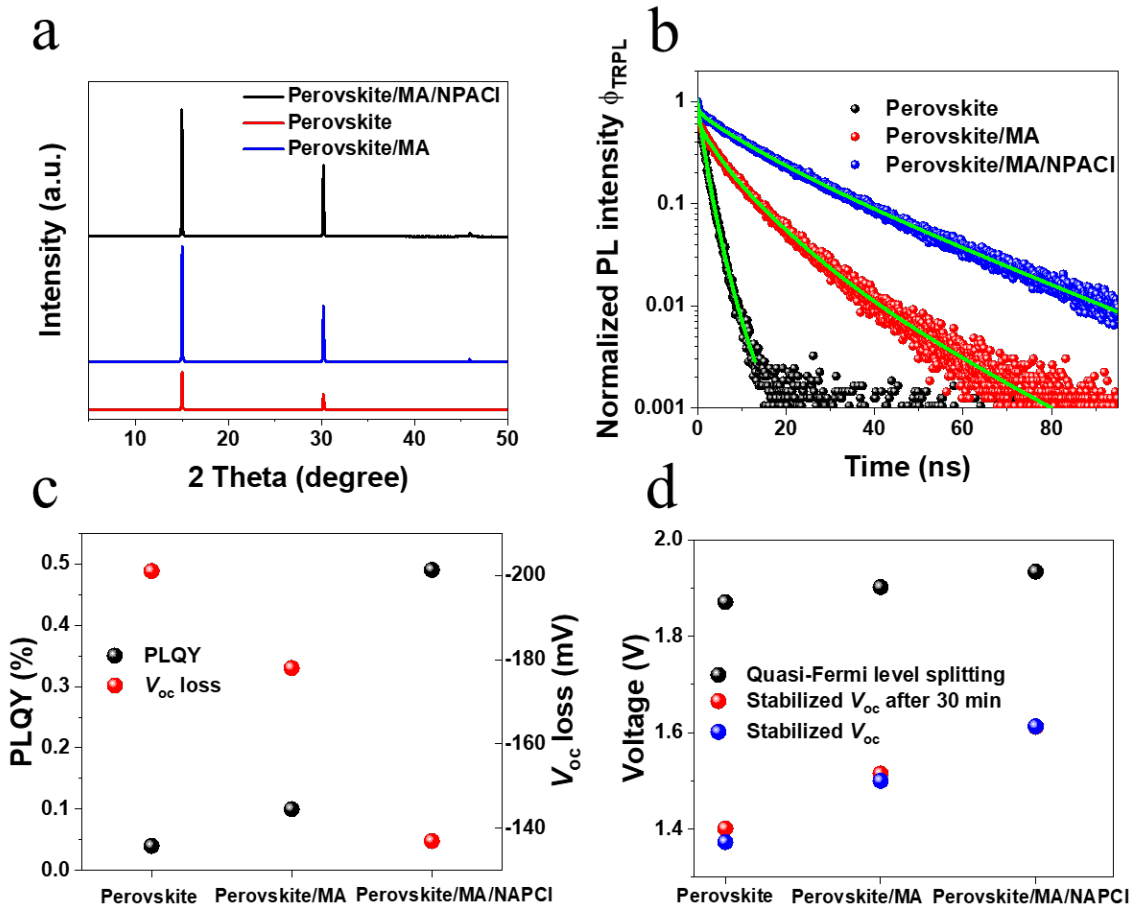

Figure 3. (a), XRD patterns of perovskite, perovskite/MA and perovskite/MA/NPACl films. (b), TRPL measurements of glass/FTO/c-TiO_2/mp-TiO_2/perovskite, perovskite/MA and perovskite /MA/NPACl. The green curves are fit curves used to calculate the differential lifetime shown in **Figure S7**. These fit curves are arbitrary functions fitting best the measured data, there is no physical meaning behind these fits. (c), PLQY and V_{oc} losses for glass/FTO/c-TiO_2/mp-TiO_2/perovskite, perovskite/MA or perovskite/MA/NPACl films. (d), Stabilized V_{oc} (1 min light soaking) and $\Delta E_F/q$ for PSCs based on pristine perovskite, perovskite/MA or perovskite/MA/NPACl. The V_{oc} of the PSCs after 30 min light soaking is also shown.

We measured the photoluminescence quantum yield (PLQY) to quantify nonradiative recombination losses in our PSCs.[35-36] **Figure 3c** shows the external PLQY ($PLQY_{ext}$) of the pristine perovskite, perovskite/MA and perovskite/MA/NPACl films determined from the absolute photon flux[37] (**Figure S3**). The $PLQY_{ext}$ of perovskite/MA is 2.5 times higher than that of the

pristine film, implying that the MA post-treatment can effectively suppress non-radiative recombination, and the PLQY of perovskite/MA/NPACl is about 5 times higher than pristine perovskite films, indicating that NPACl further inhibits non-radiative recombination. These results are in good agreement with the trends in the TRPL measurements. The resulting V_{oc} losses due to non-radiative recombination for perovskite, perovskite/MA and perovskite/MA/NPACl films are calculated by the equation $\Delta V = kT \ln(PLQY)$.[15] As shown in **Figure 3c**, the perovskite film with a NPACl layer shows a V_{oc} loss due to non-radiative recombination as small as 137 mV, compared to the control perovskite film exhibiting a V_{oc} loss of about 210 mV, allowing the devices based on perovskite/MA/NPACl to potentially afford a higher device V_{oc}. **Figure 3d** shows the measured device V_{oc} and the quasi-Fermi level splitting ($\Delta E_F/q$) calculated from the Shockley-Queisser limit of V_{oc} ($V_{oc,sq}$ = 1.98 V):[15] $\Delta E_F/q = V_{oc,sq} + \Delta V$. $\Delta E_F/q$ is the internal voltage of the absorber layer which represents the maximum V_{oc} a solar cell with this absorber can achieve. The measured device V_{oc} is significantly smaller due to energy level misalignments,[38-39] but it follows the same trend as the $\Delta E_F/q$ which shows that the V_{oc} improvements are related to the reduction of non-radiative recombination pathways. The V_{oc} after 30 min light soaking of the perovskite/MA/NPACl based device remains stable, meaning that NPACl can promote the formation of a more stable interface between the perovskite and spiro-OMeTAD.

We exploited the advantage of combining both MA vapor post-treatment and NPACl surface coating to fabricate photovoltaic cells (the cross-sectional SEM image of this device is shown in **Figure S8**, showing a dense perovskite layer of about 300 nm) for which *J-V* curves measured under standard global AM-1.5 sunlight are shown in **Figure 4a**. From this data, we derive the PV-performance metrics listed in **Table 1**. The perovskite/MA/NPACl based devices gave by far the best performance yielding a PCE of 10.33%, a FF of 71.9%, a J_{sc} of 8.71 mA cm^{-2} and a V_{oc} of 1.65 V, presenting a new record for single-junction mesoporous PSCs (NPACl can also improve FA-based wide bandgap PSCs, as shown in **Table S2**). **Figure 4b** and **S9** show the incident photon-to-electron conversion efficiency (IPCE) spectra of PSCs based on pristine perovskite and perovskite/MA/NPACl. By integrating the IPCE curves over the solar emission we calculate J_{sc} values of 6.17 and 8.38 mA cm^{-2} for the control and MA/NPACl treated perovskite respectively, in good agreement with the J_{sc} obtain from our *J-V* measurements. **Figure 4c** shows the power output at the maximum power point (MPP) for the best performing PSCs based on perovskite and perovskite/MA/NPACl under 10% relative humidity (R.H.) condition within the first 250 s. We

obtain stabilized PCEs of 10.20 and 6.06% for PSCs based on perovskite/MA/NPACl and the control, respectively, matching well the PCEs obtained from the *J-V* measurements. **Figure 4d** presents statistical data for PCE derived from measurements on 20 PSCs based on pristine perovskite and perovskite/MA/NPACl fabricated from a same batch. Statistical data on the detailed PV metrics are shown in **Figure S10**. PSCs based on perovskite/MA/NPACl exhibit good reproducibility, with an average PCE of 9.73%.

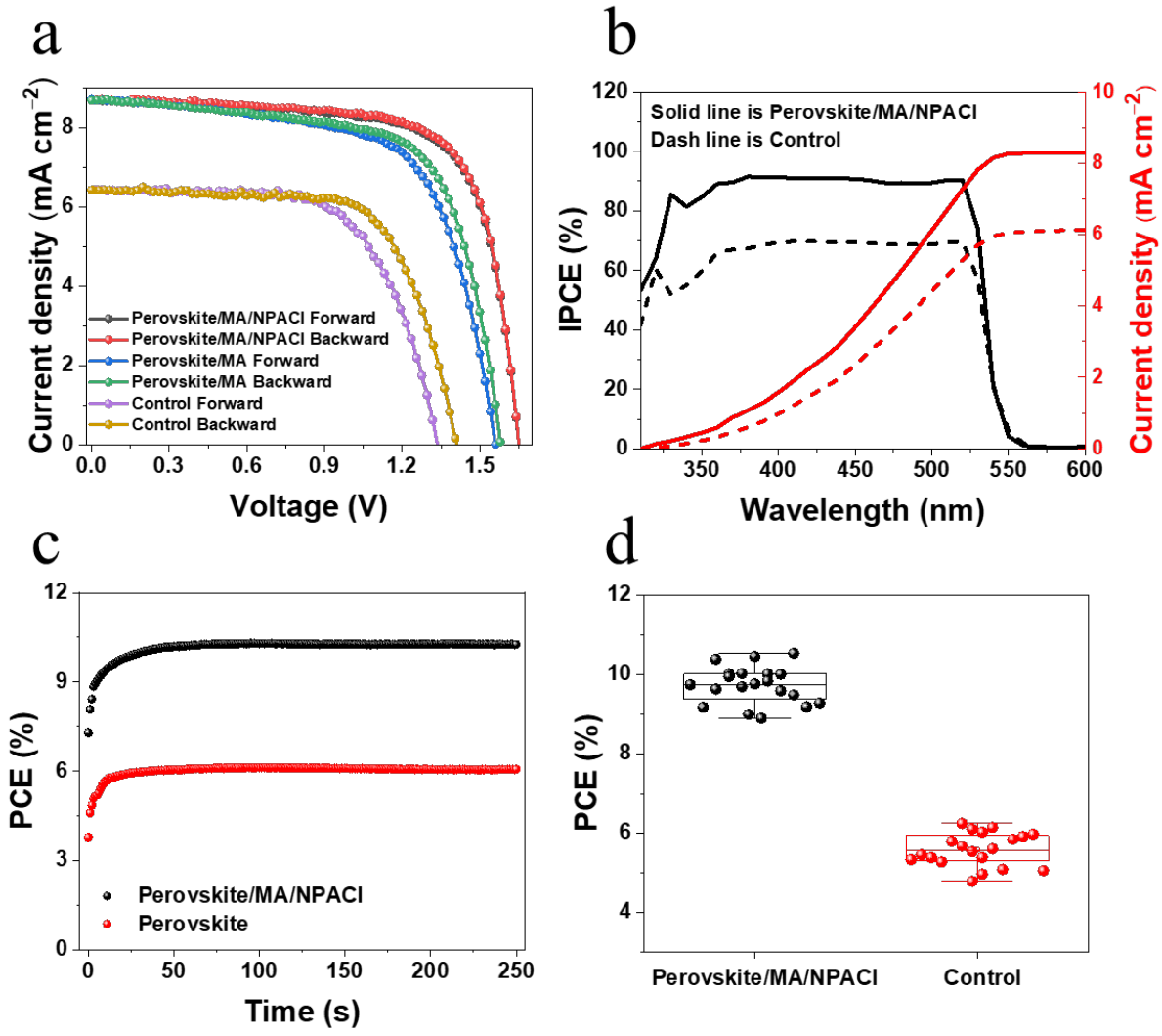

Figure 4. (a), *J–V* curves of champion devices based on control, perovskite/MA, and perovskite/MA/NPACl. (b), IPCE spectra and integrated current density values of a control PSC and a PSC based on perovskite/MA/NPACl. (c), MPP tracking of the PSCs within the first 250 s

under ambient 10% R.H. (d), PCE distributions of 20 devices obtained from perovskite and perovskite/MA/NPACl devices.

We derived the ideality factor (n_{id}) of the devices from light intensity dependent V_{oc} measurements[40] and present results in **Figure 5a** and **Figure S13a** The n_{id} of perovskite/MA/NPACl is calculated to be 1.44, which is considerably smaller than that of the control (n_{id} = 1.71) and perovskite/MA (n_{id} = 1.58), indicating that the perovskite/MA/NPACl devices show less trap-assisted non-radiative recombination,[41] which is in good agreement with the TRPL and PLQY measurements and with the better photovoltaic performance of the corresponding PSCs.

Table 1. Photovoltaic Parameters of Champion Devices based on Pristine Perovskite and Perovskite/MA/NPACl Devices Measured under Simulated AM 1.5G Irradiance.

	V_{oc} (V)	J_{sc}[a] (mA cm^{-2})	J_{sc}[b] (mA cm^{-2})	FF	PCE (%)
Perovskite/MA/NPACl Backward	1.650	8.71	8.38	0.719	10.33
Perovskite/MA/NPACl Forward	1.650	8.71		0.711	10.22
Control Backward	1.410	6.42	6.17	0.689	6.24
Control Forward	1.337	6.45		0.648	5.59

a) J_{sc} determined from the J–V measurement; b) J_{sc} determined from IPCE.

We measured the operational stability of PSCs based on pristine perovskite, perovskite/MA, and perovskite/MA/NPACl treated $MAPbBr_3$ films by tracking their maximum power point under continuous simulated 1-sun illumination, while holding the cell temperature at 60 °C. Devices were unsealed and kept under continuous nitrogen flow. Results are shown in **Figure 5b** and **S13b**. After 1100 h MPP tracking, the PSC based on perovskite/MA/NPACl retained 91% of its initial efficiency, while the PSC based on pristine perovskite retained only 34%. We attribute this dramatic improvement in the operational stability to the combined effects of the MA and NPACl treatment: MA gas post-treatment can effectively eliminate perovskite layer bulk defects and can promote the formation of a good interface between the TiO_2 layer and the perovskite layer, while NPACl can effectively reduce the concentration of perovskite surface defects and promote the formation of a strong interface between spiro-OMeTAD and the perovskite layer, resulting in a more stable perovskite structure with less ionic/defect migration. The temporal decay curves of

photovoltaic parameters including V_{oc}, J_{sc} and FF are shown in **Figure S11** and **S12**. Shelf lives were also measured by storing PSCs based on pristine perovskite, perovskite/MA, and perovskite/MA/NPACl at room temperature and ~40% R.H. in ambient air, and the results are shown in **Figure 5c** and **Figure S13c**. The superior stability of perovskite/MA/NPACl based PSCs against ambient moisture is ascribed to the stable perovskite/spiro–OMeTAD interface, fewer defects at the perovskite surface, and water rejection by the hydrophobic neopentyl moiety of NPACl (**Figure S14**).

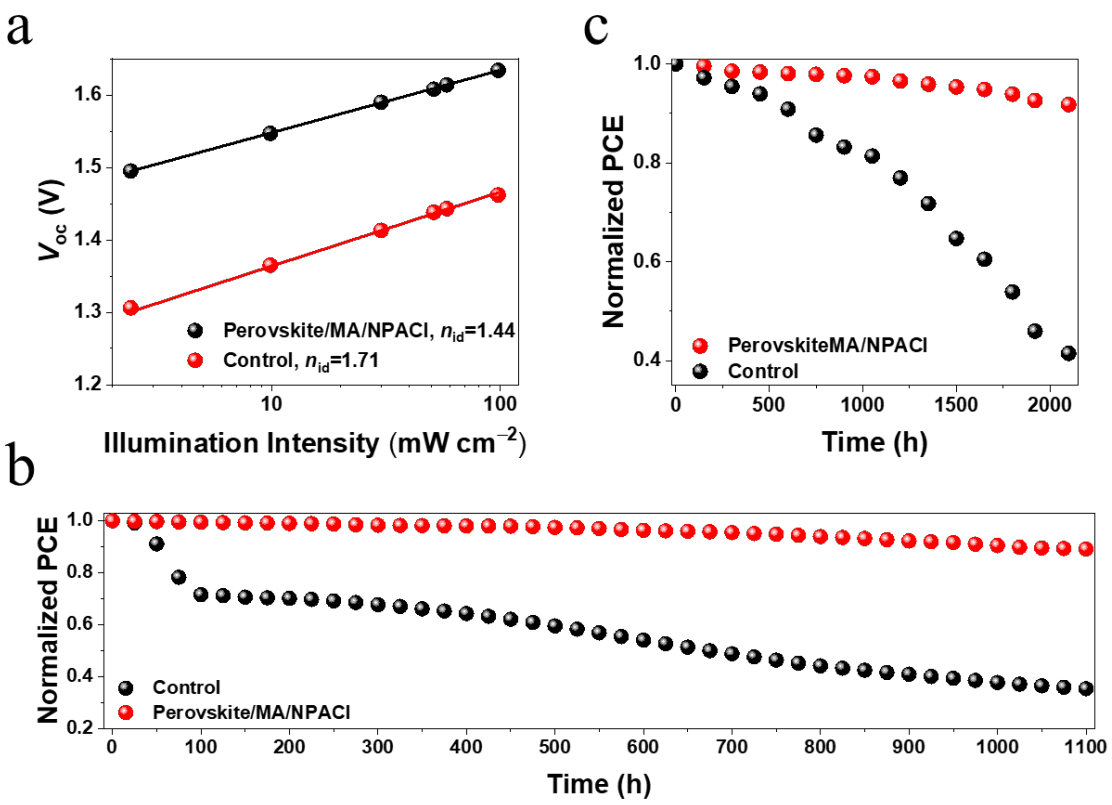

Figure 5. (a), V_{oc} as a function of light intensity of a control PSC and a perovskite/MA/NPACl based PSC with n_{id} shown in the inset. (b), MPP tracking results of a control PSC and a perovskite/MA/NPACl based PSC in inert atmosphere (N_2), 60 °C and under continuous 1-sun irradiation. (c), shelf stabilities of a control PSC and a perovskite/MA/NPACl based PSC under a R.H. of about 40%.

In conclusion, we achieved high performing $MAPbBr_3$ based PSCs with PCE over 10% and a record level V_{oc} of 1.65 V through MA vapor post-treatment in combination with surface treatment using a judiciously designed amphiphilic molecular surface modifier. In addition, we achieve outstanding operational stability under 1100 hours of simulated 1-sun illumination at 60 °C temperature. Our work provides an effective approach to realize high performance and stable $MAPbBr_3$ based large bandgap PSCs, and is of great interest for further applications such as tandem solar cells and solar water splitting.

ASSOCIATED CONTENT

Supporting Information

Experimental section and additional characterization.

Acknowledgements

H.Z. thanks the China Scholarship Council for funding. Y.L., S.M.Z., and M.G. thank the King Abdulaziz City for Science and Technology (KACST) and the European Union's Horizon 2020 research and innovation program (grant agreement No 826013) for financial support. X.L. acknowledges the financial support from the National Science Foundation of China (No. 21676188). S.W. thanks the National Key Research and Development Program of China (2016YFB0401303). M.A.H. acknowledges a Marie Skłodowska-Curie fellowship, grant number 101024144. L.E. acknowledges the Swiss National Science Foundation, grant no. 200020_178860.

AUTHOR INFORMATION

Corresponding Author

Felix Thomas Eickemeyer – *Laboratory of Photonics and Interfaces (LPI), Institute of Chemical Sciences & Engineering, École Polytechnique Fédérale de Lausanne, Lausanne 1015, Switzerland; Email: felix.eickemeyer@epfl.ch*

Yuhang Liu – *Laboratory of Photonics and Interfaces (LPI), Institute of Chemical Sciences & Engineering, École Polytechnique Fédérale de Lausanne, Lausanne 1015, Switzerland; Email: yuhang.liu@epfl.ch*

Michael Grätzel – *Laboratory of Photonics and Interfaces (LPI), Institute of Chemical Sciences & Engineering, École Polytechnique Fédérale de Lausanne, Lausanne 1015, Switzerland; Email: michael.graetzel@epfl.ch*

Authors

Hongwei Zhu – *School of Chemical Engineering and Technology, Tianjin University, Tianjin 300072, China; Laboratory of Photonics and Interfaces (LPI), Institute of Chemical Sciences & Engineering, École Polytechnique Fédérale de Lausanne, Lausanne 1015, Switzerland; Collaborative Innovation Center of Chemical Science and Engineering, Tianjin 300072, China*
Linfeng Pan – *Laboratory of Photomolecular Science (LSPM), Institute of Chemical Sciences & Engineering, École Polytechnique Fédérale de Lausanne, Station 6, Lausanne 1015, Switzerland*
Michael A. Hope – *Laboratory of Magnetic Resonance, Institute of Chemical Sciences and Engineering, École Polytechnique Fédérale de Lausanne (EPFL), Lausanne, Switzerland*
Olivier Ouellette – *Laboratory of Photonics and Interfaces (LPI), Institute of Chemical Sciences & Engineering, École Polytechnique Fédérale de Lausanne, Lausanne 1015, Switzerland*
Anwar Qasem M Alanazi – *Laboratory of Photonics and Interfaces (LPI), Institute of Chemical Sciences & Engineering, École Polytechnique Fédérale de Lausanne, Lausanne 1015, Switzerland*
Jing Gao – *Laboratory of Photonics and Interfaces (LPI), Institute of Chemical Sciences & Engineering, École Polytechnique Fédérale de Lausanne, Lausanne 1015, Switzerland*
Thomas Paul Baumeler – *Laboratory of Photonics and Interfaces (LPI), Institute of Chemical Sciences & Engineering, École Polytechnique Fédérale de Lausanne, Lausanne 1015, Switzerland*
Xiangao Li – *School of Chemical Engineering and Technology, Tianjin University, Tianjin 300072, China; Collaborative Innovation Center of Chemical Science and Engineering, Tianjin 300072, China*
Shirong wang – *School of Chemical Engineering and Technology, Tianjin University, Tianjin 300072, China; Collaborative Innovation Center of Chemical Science and Engineering, Tianjin 300072, China*
Shaik M. Zakeeruddin – *Laboratory of Photonics and Interfaces (LPI), Institute of Chemical Sciences & Engineering, École Polytechnique Fédérale de Lausanne, Lausanne 1015, Switzerland*
Lyndon Emsley – *Laboratory of Magnetic Resonance, Institute of Chemical Sciences and Engineering, École Polytechnique Fédérale de Lausanne (EPFL), Lausanne, Switzerland*

Notes

The authors declare no competing financial interest.

Reference

1. Masi, S.; Gualdron-Reyes, A. F.; Mora-Sero, I., Stabilization of Black Perovskite Phase in $FAPbI_3$ and $CsPbI_3$. *ACS Energy Lett*. **2020,** *5* (6), 1974-1985.
2. Zhu, H.; Zhang, F.; Xiao, Y.; Wang, S.; Li, X., Suppressing defects through thiadiazole derivatives that modulate $CH_3NH_3PbI_3$ crystal growth for highly stable perovskite solar cells under dark conditions. *J. Mater. Chem. A* **2018,** *6*, 4971-4980.
3. Kapil, G.; Bessho, T.; Ng, C. H.; Hamada, K.; Pandey, M.; Kamarudin, M. A.; Hirotani, D.; Kinoshita, T.; Minemoto, T.; Shen, Q.; Toyoda, T.; Murakami, T. N.; Segawa, H.; Hayase, S., Strain relaxation and light management in tin-lead perovskite solar cells to achieve high efficiencies. *ACS Energy Lett*. **2019,** *4* (8), 1991-1998.
4. Kojima, A.; Teshima, K.; Shirai, Y.; Miyasaka, T., Organometal halide perovskites as visible-light sensitizers for photovoltaic cells. *J. Am. Chem. Soc*. **2009,** *131* (17), 6050-6051.
5. Green, M. A.; Dunlop, E. D.; Hohl-Ebinger, J.; Yoshita, M.; Kopidakis, N.; Ho-Baillie, A. W. Y., Solar cell efficiency tables (Version 55). *Prog. Photovoltaics* **2020,** *28* (1), 3-15.

6. Kim, G.; Min, H.; Lee, K. S.; Lee, D. Y.; Yoon, S. M.; Seok, S. I., Impact of Strain Relaxation on Performance of α-Formamidinium Lead Iodide Perovskite Solar Cells. *Science* **2020,** *370* (6512), 108-112.
7. Yoo, J. J.; Seo, G.; Chua, M. R.; Park, T. G.; Lu, Y.; Rotermund, F.; Kim, Y.-K.; Moon, C. S.; Jeon, N. J.; Correa-Baena, J.-P.; Bulović, V.; Shin, S. S.; Bawendi, M. G.; Seo, J., Efficient perovskite solar cells via improved carrier management. *Nature* **2021,** *590* (7847), 587-593.
8. Jiang, Q.; Zhao, Y.; Zhang, X.; Yang, X.; Chen, Y.; Chu, Z.; Ye, Q.; Li, X.; Yin, Z.; You, J., Surface Passivation of Perovskite Film for Efficient Solar Cells. *Nat. Photonics* **2019,** *13*, 460-466.
9. Liu, Y.; Akin, S.; Hinderhofer, A.; Eickemeyer, F. T.; Zhu, H.; Seo, J.-Y.; Zhang, J.; Schreiber, F.; Zhang, H.; Zakeeruddin, S. M.; Hagfeldt, A.; Dar, M. I.; Graetzel, M., Stabilization of highly efficient and stable phase-pure FAPbI3 perovskite solar cells by molecularly tailored 2D-overlayers. *Angew. Chem., Int. Ed.* **2020,** *59* (36), 15688.
10. Zhu, H.; Shen, Z.; Pan, L.; Han, J.; Eickemeyer, F. T.; Ren, Y.; Li, X.; Wang, S.; Liu, H.; Dong, X.; Zakeeruddin, S. M.; Hagfeldt, A.; Liu, Y.; Grätzel, M., Low-cost dopant additive-free hole-transporting material for a robust perovskite solar cell with efficiency exceeding 21%. *ACS Energy Lett.* **2021,** *6* (1), 208-215.
11. Zhang, Y.; Seo, S.; Lim, S. Y.; Kim, Y.; Kim, S.-G.; Lee, D.-K.; Lee, S.-H.; Shin, H.; Cheong, H.; Park, N.-G., Achieving Reproducible and High-Efficiency (>21%) Perovskite Solar Cells with a Presynthesized $FAPbI_3$ Powder. *ACS Energy Lett.* **2020,** *5* (2), 360-366.
12. Zhang, F.; Lu, H.; Larson, B. W.; Xiao, C.; Dunfield, S. P.; Reid, O. G.; Chen, X.; Yang, M.; Berry, J. J.; Beard, M. C.; Zhu, K., Surface lattice engineering through three-dimensional lead iodide perovskitoid for high-performance perovskite solar cells. *Chem* **2021,** *7* (3), 774-785.
13. Wang, W.; Tadé, M. O.; Shao, Z., Research progress of perovskite materials in photocatalysis- and photovoltaics-related energy conversion and environmental treatment. *Chemical Society Reviews* **2015,** *44* (15), 5371-5408.
14. Hu, X.; Jiang, X.-F.; Xing, X.; Nian, L.; Liu, X.; Huang, R.; Wang, K.; Yip, H.-L.; Zhou, G., Wide-Bandgap Perovskite Solar Cells With Large Open-Circuit Voltage of 1653 mV Through Interfacial Engineering. *Sol. RRL* **2018,** *2* (8), 1800083.
15. Ross, R. T., Some thermodynamics of photochemical systems. *J. Chem. Phys.* **1967,** *46* (12), 4590-4593.
16. Aranda, C.; Guerrero, A.; Bisquert, J., Ionic Effect Enhances Light Emission and the Photovoltage of Methylammonium Lead Bromide Perovskite Solar Cells by Reduced Surface Recombination. *ACS Energy Lett.* **2019,** *4* (3), 741-746.
17. Wu, C.-G.; Chiang, C.-H.; Chang, S. H., A perovskite cell with a record-high-Voc of 1.61 V based on solvent annealed $CH_3NH_3PbBr_3$/ICBA active layer. *Nanoscale* **2016,** *8* (7), 4077-4085.
18. Singh, S.; Kabra, D., Influence of solvent additive on the chemical and electronic environment of wide bandgap perovskite thin films. *J. Mater. Chem. C* **2018,** *6*, 12052-12061.
19. Shao, Z.; Wang, Z.; Li, Z.; Fan, Y.; Meng, H.; Liu, R.; Wang, Y.; Cui, G.; Hagfeldt, A.; Pang, S., A scalable methylamine gas healing strategy for high efficiency inorganic perovskite solar cells. *Angew. Chem. Int. Ed.* **2019,** *58*, 5578.
20. Zhang, M.-J.; Wang, N.; Pang, S.-P.; Lv, Q.; Huang, C.-S.; Zhou, Z.-M.; Ji, F.-X., Carrier transport improvement of $CH_3NH_3PbI_3$ film by methylamine gas treatment. *ACS Appl. Mater. Interfaces* **2016,** *8* (45), 31413-31418.
21. Raga, S. R.; Ono, L. K.; Qi, Y., Rapid perovskite formation by CH3NH2 gas-induced intercalation and reaction of PbI2. *J. Mater. Chem. A* **2016,** *4* (7), 2494-2500.

22. Li, C.; Pang, S.; Xu, H.; Cui, G., Methylamine Gas Based Synthesis and Healing Process Toward Upscaling of Perovskite Solar Cells: Progress and Perspective. *Sol. RRL* **2017,** *1* (9), 1700076.
23. Liu, J.; Leng, J.; Wang, S.; Zhang, J.; Jin, S., Artifacts in Transient Absorption Measurements of Perovskite Films Induced by Transient Reflection from Morphological Microstructures. *J. Phys. Chem. Lett.* **2019,** *10* (1), 97-101.
24. Krueckemeier, L.; Rau, U.; Stolterfoht, M.; Kirchartz, T., How to Report Record Open-Circuit Voltages in Lead-Halide Perovskite Solar Cells. *Adv. Energy Mater.* **2020,** *10*, 1902573.
25. Zhu, H.; Ren, Y.; Pan, L.; Ouellette, O.; Eickemeyer, F. T.; Wu, Y.; Li, X.; Wang, S.; Liu, H.; Dong, X.; Zakeeruddin, S. M.; Liu, Y.; Hagfeldt, A.; Gratzel, M., Synergistic Effect of Fluorinated Passivator and Hole Transport Dopant Enables Stable Perovskite Solar Cells with an Efficiency Near 24%. *J. Am. Chem. Soc.* **2021,** *143* (8), 3231-3237.
26. Reif, B.; Ashbrook, S. E.; Emsley, L.; Hong, M., Solid-state NMR spectroscopy. *Nature Reviews Methods Primers* **2021,** *1* (1), 2.
27. Kubicki, D. J.; Stranks, S. D.; Grey, C. P.; Emsley, L., NMR spectroscopy probes microstructure, dynamics and doping of metal halide perovskites. *Nature Reviews Chemistry* **2021,** *5* (9), 624-645.
28. Alharbi, E. A.; Alyamani, A. Y.; Kubicki, D. J.; Uhl, A. R.; Walder, B. J.; Alanazi, A. Q.; Luo, J.; Burgos-Caminal, A.; Albadri, A.; Albrithen, H.; Alotaibi, M. H.; Moser, J.-E.; Zakeeruddin, S. M.; Giordano, F.; Emsley, L.; Gratzel, M., Atomic-level passivation mechanism of ammonium salts enabling highly efficient perovskite solar cells. *Nat. Commun.* **2019,** *10* (1), 3008.
29. Krishna, A.; Akhavan Kazemi, M. A.; Sliwa, M.; Reddy, G. N. M.; Delevoye, L.; Lafon, O.; Felten, A.; Do, M. T.; Gottis, S.; Sauvage, F., Defect Passivation via the Incorporation of Tetrapropylammonium Cation Leading to Stability Enhancement in Lead Halide Perovskite. *Adv. Funct. Mater.* **2020,** *30* (13), 1909737.
30. Franssen, W. M. J.; Bruijnaers, B. J.; Portengen, V. H. L.; Kentgens, A. P. M., Dimethylammonium Incorporation in Lead Acetate Based MAPbI3 Perovskite Solar Cells. *ChemPhysChem* **2018,** *19* (22), 3107-3115.
31. Han, L.; Liu, C.; Wu, L.; Zhang, J., Growth of $MAPbBr_3$ single-crystalline thin film based on space-limited method. *J. Cryst. Growth* **2018,** *501*, 27-33.
32. Noel, N. K.; Wenger, B.; Habisreutinger, S. N.; Patel, J. B.; Crothers, T.; Wang, Z.; Nicholas, R. J.; Johnston, M. B.; Herz, L. M.; Snaith, H. J., Highly Crystalline Methylammonium Lead Tribromide Perovskite Films for Efficient Photovoltaic Devices. *ACS Energy Lett.* **2018,** *3* (6), 1233-1240.
33. Kirchartz, T.; Marquez, J. A.; Stolterfoht, M.; Unold, T., Photoluminescence-Based Characterization of Halide Perovskites for Photovoltaics. *Adv. Energy Mater.* **2020,** *10*, 1904134.
34. Krückemeier, L.; Krogmeier, B.; Liu, Z.; Rau, U.; Kirchartz, T., Understanding Transient Photoluminescence in Halide Perovskite Layer Stacks and Solar Cells. *Advanced Energy Materials* **2021,** *11* (19), 2003489.
35. Motti, S. G.; Meggiolaro, D.; Barker, A. J.; Mosconi, E.; Perini, C. A. R.; Ball, J. M.; Gandini, M.; Kim, M.; De Angelis, F.; Petrozza, A., Controlling competing photochemical reactions stabilizes perovskite solar cells. *Nat. Photonics* **2019,** *13*, 532-539.
36. Luo, D.; Su, R.; Zhang, W.; Gong, Q.; Zhu, R., Minimizing Non-radiative Recombination Losses in Perovskite Solar Cells. *Nat. Rev. Mater.* **2019,** *5*, 44-60.

37. de Mello, J. C.; Wittmann, H. F.; Friend, R. H., An improved experimental determination of external photoluminescence quantum efficiency. *Adv. Mater.* **1997,** *9*, 230-232.
38. Caprioglio, P.; Stolterfoht, M.; Wolff, C. M.; Unold, T.; Rech, B.; Albrecht, S.; Neher, D., On the relation between the open-circuit voltage and quasi-fermi level splitting in efficient perovskite solar cells. *Adv. Energy Mater.* **2019,** *5*, 1901631.
39. Ahangharnejhad, R. H.; Friedl, J. D.; Phillips, A. B.; Heben, M. J., Understanding V_{OC} and performance deficit in wide bandgap perovskite photovoltaic devices. *Sol. Energy Mater Sol. Cells* **2021,** *225*, 111015.
40. Tress, W.; Yavari, M.; Domanski, K.; Yadav, P.; Niesen, B.; Correa Baena, J. P.; Hagfeldt, A.; Graetzel, M., Interpretation and evolution of open-circuit voltage, recombination, ideality factor and subgap defect states during reversible light-soaking and irreversible degradation of perovskite solar cells. *Energy Environ. Sci.* **2018,** *11* (1), 151-165.
41. Wu, W.-Q.; Yang, Z.; Rudd, P. N.; Shao, Y.; Dai, X.; Wei, H.; Zhao, J.; Fang, Y.; Wang, Q.; Liu, Y.; Deng, Y.; Xiao, X.; Feng, Y.; Huang, J., Bilateral alkylamine for suppressing charge recombination and improving stability in blade-coated perovskite solar cells. *Sci Adv* **2019,** *5* (3), eaav8925.

TOC: